Thermal neutron measurement by single crystal CVD diamond detector applied with the pulse shape discrimination during deuterium plasma experiment in LHD

Makoto I. Kobayashi[1,2], Maurizio Angelone[1,3], Sachiko Yoshihashi[4], Kunihiro Ogawa[1,2], Mitsutaka Isobe[1,2], Takeo Nishitani[1], Siriyaporn Sangaroon[1], Shuji Kamio[1], Yutaka Fujiwara[1], Tomomi Tsubouchi[2,5], Akira Uritani[4], Minoru Sakama[6], Masaki Osakabe[1,2], and the LHD Experiment Group[1]

1. National Institute for Fusion Science, National Institutes of Natural Sciences, Toki, Gifu, Japan
2. The Graduate University for Advanced Studies, SOKENDAI, Toki, Gifu, Japan
3. ENEA, Fusion and Technology for Nuclear Safety and Security Department, C.R. Frascati, via E. Fermi 45, 00044 Frascati, Italy
4. Nagoya University, Nagoya, Aichi, Japan
5. National Institute for Basic Biology, National Institutes of Natural Sciences, Okazaki, Aichi, Japan
6. Tokushima University, Tokushima, Japan

Abstract

The Pulse shape discrimination (PSD) technique for single crystal CVD diamond detector (SDD) was applied to the real-time thermal neutron measurement during the 3rd campaign of Deuterium-Deuterium (D-D) plasma experiment in the Large Helical Device (LHD). The PSD method is based upon the different shape of electrical pulses produced in diamond by gamma-ray (triangular-shaped pulse) and energetic ions (rectangular-shaped pulse), respectively. An improved PSD was developed which makes use of the full width at half maximum (FWHM) and the full width at 2/3 of the peak height (FW2/3PH). These two parameters reflect the difference in the pulse shape produced by gamma-rays and energetic ions.

The performance of this improved PSD technique was first tested irradiating the SDD by gamma-rays from ^{60}Co and alphas from ^{241}Am radiation sources, respectively. Then, using a ^{6}LiF thermal neutron converter, a successful discrimination between gamma-rays and alpha particles and tritons generated by the $^{6}Li(n,\alpha)^{3}H$ reaction induced by neutrons from ^{252}Cf spontaneous fission neutron source was achieved. Thanks to this PSD processing technique, the thermal neutron detection efficiency increased about 1.7 times compared to previous measurements performed without the PSD technique.

The real-time thermal neutron measurement by SDD with this enhanced PSD processing was also used during D-D plasma discharges in the Large Helical Device (LHD). It was found that both the time integrated counts and the time evolution count rate measured by the SDD reproduced well that of the fission chamber used as official LHD neutron monitor. The capability of the SDD detector using the PSD technique of precise real-time thermal neutron measurement in LHD was demonstrated.

Keyword

Single crystal CVD diamond detector, thermal neutron, pulse shape discrimination, gamma-ray

1. Introduction

In the fusion experiments using deuterium-deuterium (D-D) and/or deuterium-tritium plasma (D-T), the precise measurement of the emitted neutrons is very important for both the physics research and the radiation safety [1-5]. Neutron interaction with materials is significantly dependent upon the neutron energy [6] and proper neutron detectors must be selected depending upon the neutron energy range to be investigated. Furthermore, the neutron detector is exposed to gamma-rays which are always associated to neutron fluxes. Therefore, insensitivity to or discrimination property for gamma-rays are thus the essential criterion for selecting the proper neutron detector to attain reliable measurements of the neutron field.

Single crystal diamond (SCD) is an attractive material as neutron detector because of its advantages such as fast neutron detection capability, small size, intrinsic low sensitivity to gamma-rays (due to its small atomic number), high radiation tolerance, high temperature operation capability, needless of cryogenic system, and others [7-8]. Diamond is mainly sensitive to fast neutrons via elastic collisions and $^{12}C(n,x)$ reactions [9]. Although diamond is not sensitive to thermal neutrons, the use of a thermal neutron converter such as lithium or boron allows SCD to detect thermal neutrons, too. In this case, energetic ions (EI) are generated by means of the (n, α) reactions induced by thermal neutrons with ^{6}Li and ^{10}B isotopes:

$$^{6}Li(n,\alpha)^{3}H\ ; \quad \alpha = 2.0\ MeV, \quad ^{3}H = 2.7\ MeV$$
$$^{10}B(n,\alpha)^{7}Li, \quad \alpha = 1.5\ MeV\ ;\ ^{7}Li = 0.8\ MeV$$

By putting a thermal neutron converter on a surface of the SCD, the produced EI injects into the SCD. The slowing-down of these EI inside the SCD produces a significant amount of hole-electron (h-e) pairs which induce electrical pulses at the detector's electrodes, thus indicating the neutron detection [10, 11]. Diamond detectors covered with ^{6}LiF were used many years for neutron detection [10, 12, 13] in different applications. The first application to the time dependent neutron emission from fusion machines was at the Joint European Tokamak (JET) in the 2006-2007 D-D campaign [14]. Recently, other measurements in fusion experimental devices such as EAST and HL-2A were reported too [15, 16]. Like these experiments, the capability of diamond detectors for measuring fast neutron and thermal neutron fluxes simultaneously without a large influence on the neutron field (due to small size) at high temperature is the most attractive characteristic compared to other radiation detectors in the fusion research field.

In the Large Helical Device (LHD), which is one of the world's largest superconducting "stellarator" type fusion machines, D-D plasma experiment initiated in March 2017 [17-19]. One single crystal CVD diamond detector (SDD) was installed and used in the LHD torus hall during the 2nd campaign of the D-D experiment with the goal to measure and characterize the neutron flux [20]. This SDD was made with a SCD with the thickness of 140 μm, and covered by a 1.9 μm-thick ^{6}LiF foil. The use of a thin SCD aimed to decrease the detection efficiency for gamma-rays. Additionally, in the attempt to reduce the gamma contamination of the measurements, the detector was used by setting a high threshold level to cut low energy signals produced by gamma-ray. Therefore, this method leads also to cut pulses induced by the slowed-down ions, which resulted in the decrease of detection efficiency to thermal neutrons.

The thermal neutron detection efficiency of SDD can be improved if the signals due to the slowed-down ions could be extracted from the "background" signal produced by gamma-rays. To this purpose, the pulse shape discrimination (PSD) technique already applied to diamond detector in [21] was applied also in this study.

The PSD method used in this work was an improved version with respect to that used in [21] because we developed a multi-filtering scheme based upon both the full width at half maximum (FWHM) and the full width at 2/3 of the peak height (FW2/3PH). This allows a more accurate discrimination among the signals due to EI, gamma-rays as well as the electrical noises.

In order to test and assess this improved PSD method, its performance and effectiveness were first studied by irradiating the SDD with gamma-rays and alpha-rays using radiation sources. Then, the test was performed using ^{6}LiF thermal neutron converter by exposing the SDD to the neutron field by a ^{252}Cf spontaneous fission neutron source to which a not negligible prompt gamma-ray field is associated. After these performance tests, the PSD method was, for the first time ever, applied to the real-time thermal neutron measurement during the 3rd D-D plasma experiment campaign at LHD. The results of the measurements with the SDD operated with the PSD technique were thus compared to the ^{235}U fission chamber (FC) used as LHD official neutron monitor.

2. Pulse shape discrimination

2.1 Difference of pulse shape induced by radiations

The pulse shape discrimination was carried out using the width of a pulse. In the SCD, different ionizing particles induce different pulse shapes at the electrodes [21].

In the case of EI injection into one side of the SCD (the one where the ^{6}LiF layer is located), the h-e pairs produced by the ionization inside the SCD distribute close to the

injecting surface region. Given that a positive voltage is applied on this surface, the generated holes drift toward the backside electrode of the SCD (which is grounded), while the electrons are collected by this positive electrode. The current is induced in the electrode by the charge drift in SCD according to the Schockley-Ramo theorem [22, 23]. Thus, an almost constant current is induced until all holes reach the grounded electrode. Then, a quick decrease of current will be observed due to the outflow of holes to the backside surface electrode. Consequently, a rectangular-shaped pulse will be obtained in the case of EI injection.

Besides, in the case of gamma-ray irradiation, the distribution of h-e pairs generated by scattered electrons produced by the gamma-ray (e.g., Compton electrons) is homogeneous inside the SCD. Then, the number of drifting h-e pairs in the SCD gradually decreases due to the outflow of them from both electrodes. Consequently, a triangular-shaped pulse is obtained [24].

An example showing the difference in the pulse shape induced by EI and gamma-rays is displayed in Fig. 1 where typical pulses due to alpha-ray from ^{241}Am ($E_\alpha \sim 5.5$ MeV) and gamma-ray from ^{60}Co ($E_\gamma = 1.17, 1.33$ MeV) [25] are shown. The background noise level was evaluated by the signal before and after the pulse, and already subtracted in this figure. The set-up for this measurement can be found in section 3.1. As shown in this figure, the pulse shapes induced by gamma and alpha radiations are different. The difference in the shapes of the pulses induced by EI and gamma-ray results in the difference in the width of the pulse. Therefore, the PSD was first carried out using just the FWHM of pulses [21]. In this study, the PSD method adopted not only the FWHM as in [21] but also a second parameter, the full width at 2/3 of the peak height (FW2/3PH). This improves the separation accuracy between the two different pulses.

2.2 PSD method

According to Fig. 1, each pulse (regardless if triangular or rectangular) is several ns wide. This is due to the drift velocity of the h-e carriers. Therefore, since the sampling rate of the digitizer used in this study for recording the pulses was 1 GHz (see section 3.1), the discrete data grid with 1 ns time-bin is insufficient for precise pulse analysis by PSD method because the recorded pulse is represented by a few data points (see Fig. 1). Therefore, a spline interpolation was applied to each pulse to increase the number of data points representing each pulse. The interpolated data points are shown in Fig. 1, too. By this step, the number of data points was 10 times larger than the raw data. Then, the peak-top time and the FWHM of each pulse were evaluated. The method to evaluate the FWHM of a pulse is as follows. After finding a peak-top time, the height at this position

(maximum height) was evaluated. Then, all data of each single pulse event were subtracted by the half value of the maximum height. By this subtraction, the height at half-maximum should be close to zero. Then, last and first data points with the absolute value of height close to zero just before and after the peak-top were searched, respectively. The time difference between these two points corresponds to the FWHM of the pulse. An example of the histogram of the FWHM distribution as obtained using all the recorded pulses for our SDD irradiated separately by alpha-rays from ^{241}Am and gamma-rays from ^{60}Co is shown in Fig. 2(a) (see the detector set-up in section 3.1). In this measurement, the count rates and total numbers of pulse for alpha-ray and gamma-ray were 19 cps and 30 cps, and ~24000 (measurement for 1200 s) and ~110000 (measurement for 3600 s), respectively. The bin-size of this histogram is 0.33 ns. The histogram of the FWHM shows two peaks, which are associated to gamma-ray and alpha-ray, respectively. Setting a threshold for the FWHM at 6 ns allows to separate signals due to alpha-rays from those due to gamma-rays. This figure also indicated that the FWHM of 8 ns should be an upper limit for the pulses induced by EI.

Furthermore, the radiation measurements always need to take care of the fluctuation of signals due to the noise. In particular, for the low-height pulses induced either by gamma-rays or slowed-down EI, the signal is sometimes largely fluctuated by the noise. It could happen due to noise that a signal induced by gamma-ray has amplitude above the FWHM threshold set to discriminate EI and gamma-ray. Therefore, this is leading to the misjudgment of gamma pulses as slowed-down ions. To avoid this error, a second parameter, the FW2/3PH, was also evaluated for each pulse. Fig. 2(b) reports the histogram of the FW2/3PH distribution as measured for the same measurement already shown in Fig. 2(a). The shape of the FW2/3PH histogram is similar to that of the FWHM histogram although the time duration (width) for both the EI and the gamma signals is shorter. The FW2/3PH of EI induced pulse is in the 5 ~ 6.5 ns range and can be used as a second parameter to extract the pulses due to EI from that due to gamma-rays.

The flowchart of this enhanced PSD method is shown in Fig. 3. The algorithm in this PSD method was written in Python [26]. The figures and the results reported in this paper are the output of this program.

3. Test and assessment of the PSD method

3. 1 Measurements for radiation sources

Before installing the SDD inside the LHD torus hall, different tests were performed to validate and assess the method discussed above. The detector was irradiated by gamma-rays, alpha-rays, and neutrons using sealed radiation sources.

The SDD (B12 Knopf Detector) was purchased from Cividec instrumentation GmbH [27]. The SCD is a single crystal electronic grade chemical vapor deposition diamond. The size of SCD was 4 mm × 4 mm, and the thickness was 500 μm. The major impurity concentration such as nitrogen is less than 5 ppb. A 100 nm-thick titanium layer was deposited on both SCD surfaces, thus forming the metal electrodes. The signal produced by the SDD was sent to a pre-amplifier (C2-HV broadband Amplifier of CIVIDEC) [27]. The amplified signal was recorded by DAQ system (APV8102-14MWPSAGb) composed of fast processing ADC and FPGA system with sampling rate of 1 GHz and the resolution of 14 bit [28]. Each pulse event data consisted of 64 data points (64 ns in total) including a pulse and the background signals before and after the pulse.

The ^{6}LiF layer used as thermal neutron converter was placed in air at 2 mm away from one of the electrodes of the SCD. This ^{6}LiF layer was removable, 1.9 μm thick and 4 mm diameter. Lithium was enriched in ^{6}Li at 95% by weight. When performing gamma-ray and alpha-ray irradiations, the ^{6}LiF thermal neutron converter was removed.

A 0.76 MBq ^{60}Co gamma-ray source was used for gamma-ray irradiation. For the alpha-ray irradiation, a ~550 Bq ^{241}Am alpha source was used. This source has a thin ^{241}Am layer deposited on the surface of a metal substrate. The ^{241}Am alpha-ray source was placed in the air and approximately 2 mm away from the SCD. The ^{60}Co gamma-ray source was placed approximately 2 cm away from the SCD. A bias voltage of -400 V was applied to the detector for all the various measurements reported here after.

For the neutron irradiation, a 260 MBq ^{252}Cf spontaneous neutron source was used. This corresponds to a neutron emission rate of 4.4×10^{7} s^{-1}. The ^{252}Cf spontaneous neutron source was sealed in a 1.5 mm thick stainless steel casing, and stored in the storage box made of lead, polyethylene and concrete in order to slow-down the emitted fast neutrons to thermal neutron and also to shield the strong gamma-ray field associated to the ^{252}Cf neutron emission. The SDD equipped with the ^{6}LiF converter was exposed to neutrons leaking from the ^{252}Cf storage box. The distance between the SDD and the storage box was 25 cm.

3.2 Results of the performance tests with alpha-ray, gamma-ray and neutrons

The FWHM and FW2/3PH of all pulses induced by gamma-ray and alpha-ray individual irradiation into the detector were first evaluated by the PSD method and the distribution histograms are displayed as Figs. 2(a) and 2(b), respectively. The developed algorithm for PSD also allows to calculate the total charge of each pulse, which is evaluated as an integral of current after background subtraction over a single pulse event (The integral of

64 data points as explained in section 3.1). The total charge is proportional to the deposited energy into SCD from a particular type of radiation, and widely used to identify the energy of EI injected into the detector [29]. The histogram of the total charge is shown in Fig. 4. The bin-size of this figure is 3×10^{-3} (arbitrary unit). The gray-line of this figure is the histogram of the total charge of all pulses without PSD processing. The histogram shows two peaks. The energy of alpha-ray from ^{241}Am is much higher than that of gamma-ray from ^{60}Co. In addition, only a fraction of the gamma-ray energy is transferred to SCD while almost all the energy of alpha-ray is deposited inside the SCD due to the strong interaction of charged ions in solid materials (the range of ^{241}Am alphas in Carbon is about 17 microns). Therefore, in Fig. 4, the peak with smaller total charge region should be attributed to gamma-ray while the peak with greater total charge region should be due to alpha-ray. All the pulses were analyzed by using our PSD method, and the resulting total charge histograms for gamma-rays and alpha-rays can be found in Fig.4 as blue and red curves, respectively. The total charge histograms of gamma-rays and alpha-rays were consistent with the above assignment for each peak.

The pulses induced during the neutron irradiation into the SDD with ^{6}LiF thermal neutron converter by ^{252}Cf were also analyzed with the enhanced PSD method. The histogram of total charge for all measured pulses is displayed in Fig. 5(a) as a gray curve. In this figure, the total charge is converted to the deposited energy using the conversion factor obtained from alpha-ray measurement in Fig. 4. The bin-size of this histogram is ~0.05 MeV. For Figs. 5(a), the total count number was ~78000 for measurement lasting ~60500 s, corresponding to a count rate of ~1.3 cps. The histogram of all pulses before PSD processing (gray curve) shows a high and wide peak in the low deposited energy region (< 0.2 MeV). Also, a small peak was observed in the high deposited energy region (2.2~3.2 MeV). Therefore, the recorded spectrum is clearly the superposition of different contributions from gamma-rays, EI and neutrons interacting directly in the SCD. The results of the PSD are also shown in Figs. 5(a) (red and blue curves). According to these results, most of the pulses in the low energy region were attributed to gamma-rays (blue line). Note that the pulses in the low energy region would also be induced not only by gamma-ray but also by neutrons. The neutron energy spectrum from ^{252}Cf neutron source is usually modeled as a Maxwellian distribution with the average energy of 2.14 MeV [30]. Below 5.7 MeV neutrons are interacting with carbon mainly by elastic collisions and the pulses are produced by the ionization induced by the recoiling carbon nuclei. According to [31], when neutrons interact in the bulk of the SCD, the induced current will be rectangular-shaped pulse or step-like shaped pulse with smaller FW2/3PH or FWHM than the threshold, respectively. Therefore, the pulse induced by neutrons would

be similar to the pulse by gamma-ray. The separation of pulses induced by gamma-ray and fast neutrons is still incomplete in the present PSD method. Nevertheless, the superposition of pulses induced by gamma-rays and neutrons in low deposited energy region would not impact on the detection efficiency of thermal neutron.

The two peaks in the higher deposited energy region in Figs. 5(a) were attributed to the pulses induced by EI (red line). Indeed, the $^{6}Li(n,\alpha)^{3}H$ reaction produces triton and alpha particles with kinetic energies of 2.7 MeV and 2.0 MeV, respectively. Therefore, the peak with deposited energy approximately 2.7 MeV is caused by tritons, and the peak with less energy is due to alpha particles (see Figs. 5). In the histogram, the peak area due to alpha particles was smaller compared to that due to tritons although the same number of these particles generate simultaneously in $^{6}Li(n,\alpha)^{3}H$ reaction. This should be caused by the more effective slowing-down of alpha particles in the ^{6}LiF thermal neutron converter, the air region between ^{6}LiF and SCD, and the Ti electrode due to their larger mass and charge compared to triton. The deposited energy of alpha particles was less than its original recoil energy of 2.0 MeV. This would be caused by the effective slowing-down of alpha particle before depositing into SCD and the background signal subtraction due to small pulse height by alpha particles.

The detection efficiency of thermal neutron by SDD could be increased by the PSD method, because it allows for the detection of both alpha and triton particles, compared to the previous case in ref.[16] in which only tritons were counted. This improvement of detection efficiency for thermal neutron thanks to the PSD method applied here will be further discussed in the next section.

To test the sensitivity of our algorithm to small variation of the radiation field, another measurement in the ^{252}Cf neutron field was performed by interposing 1.0 mm-thick lead shield between the storage box of ^{252}Cf neutron source and the ^{6}LiF thermal neutron converter. It is well known that lead is an effective gamma-ray shielding material. The 1.0 mm-thick lead can be an effective shielding for the gamma-ray with little change of neutron field for SDD. The histogram of deposited energy in this case is shown in Figs. 5(b). For these figures, the total count number was ~69000 in the measurement duration of ~83600 s, corresponding to the count rate of ~0.82 cps. The area in the lower energy region induced by gamma-ray has decreased to around 60% compared to that in Figs. 5(a). On the other hand, the peaks due to alpha particles and triton did not decrease compared to that in Figs. 5(a). This was expected since a thin lead layer scarcely affects the neutron flux. This was also verified by Monte Carlo simulation of the irradiation facility which demonstrated that the thermal neutron flux region was not modified by the 1 mm lead layer. The results in Figs. 5(b) confirmed the good performance of PSD algorithm

developed in this work.

3.3 Improvement of thermal neutron detection using the FW2/3PH parameter

The detection efficiency of thermal neutron will be overestimated if the PSD method cannot extract the pulses due to alpha particles from large number of pulses induced by gamma-ray, because both are in the similar energy region. To do this as accurate as possible, the FW2/3PH parameter was adopted in this work in addition to FWHM which has been used previously in [21]. The effect on the discrimination capability by this additional parameter was evaluated as a test of its effectiveness. Figure 6 shows the comparison of two cases of the energy spectra produced by EI during neutron irradiation extracted by the two different PSD methods. The red line was processed by PSD method used in this work (it is the same as in Figs. 5(a)). The green line was obtained by PSD adopting only the FWHM in the same measurement. Although the peak of triton was the same in these two cases, the peak of alpha particles was clearly larger in the case using only the FWHM. This increase in the count rate of supposing alpha particles was due to the contamination of gamma-ray induced pulses. Because of the low pulse height of such a pulse, it is easily affected by the noise, resulting in a fluctuation of pulse shape. Some examples of pulse measured during gamma-ray irradiation by ^{60}Co are shown in Fig. 7. The pulse shape is not just a simple triangular shaped pulse but shows a further smaller peak just after the peak-top. According to the PSD method using only FWHM, this pulse can be regarded as a pulse induced by EI. The improved PSD method used in this work can eliminate these “wrong” pulses due to the differences in the FW2/3PH. Compared to the PSD method using only the FWHM, about 30% of pulses were rejected using also the FW2/3PH parameter (Fig. 6). The same behavior was observed when the PSD using only FW2/3PH was applied. An example of pulse induced by gamma-ray irradiation by ^{60}Co is also displayed in Fig. 7. Due to a small (but larger than FW2/3PH) peak after the peak-top, this pulse can be regarded as a pulse induced by EI using the PSD based only on FW2/3PH although the FWHM of this pulse does not exceed the threshold FWHM value. Combining the use of FWHM and FW2/3PH can suppress the misjudgment of pulses like this case.

By the improved PSD method, the detection of slowed-down alpha particles is reliable for evaluating the thermal neutron detection efficiency of SDD. In the previous work where PSD method was not applied [16], the thermal neutron detection efficiency was only done by counting the number of pulses above the threshold for the total charge so to extract the pulses produced by tritons (The region colored in black in Fig. 8). Compared to this old method, this work could improve the detection efficiency for thermal neutron

because the pulses produced by slowed-down alpha particles were reliably included (The region colored in red in Fig. 8). According to this comparison, the thermal neutron detection efficiency increased about 1.7 times by using the new PSD method proposed in this work compared to the old one.

4. Real-time thermal neutron measurement in the LHD torus hall

Once the tests of the PSD method were completed, the SDD was installed inside the LHD torus hall, close to the pneumatic tube-end in front of 10-O port. The tube-end is on the equatorial plane of plasma, which is 5.5 m of height from the floor level of the torus hall, and about 3 m away from the surface of the cryostat of LHD. The detail of the position of the pneumatic tube-end is described in a previous work [32]. The SDD (B6-C compact thermal-neutron diamond detector) from Cividec instrumentation GmbH [27] was used. This detector also equips the ^{6}LiF thermal neutron converter with the thickness of 1.9 μm. The EI generated in ^{6}LiF layer transports and deposits energy into SCD via the window with a diameter of 3.6 mm. The distance between SCD and ^{6}LiF is 1.0 mm. Also, in this case, the detector was operated with the same pre-amplifier (C2-HV broadband Amplifier of CIVIDEC) at -400 V bias voltage. The voltage was applied to the detector prior to the start-up of experiments in LHD by an automatic switching system. The signal from the SDD was measured in real-time acquisition mode with a digitizer with sampling rate of 1 GHz. The signals recorded during each D-D discharge were transferred to the DAQ system for post-acquisition analysis as discussed above. Measurements were performed from LHD shot #154544 to #154700.

Figure 9 shows the sum of triton and alpha events obtained with the PSD method for the mentioned LHD shots as a function of neutron yield (Y_n). The neutron yield in each plasma discharge was evaluated by the neutron flux monitor using a fission chamber (FC) [33]. The maximum total count number in these data is ~11600 at Y_n = ~1.5×10^{15} n. The count rate at the data is ~ 5000 cps. Note that the total count number and count rate here include not only the events by triton and alpha particles but also by gamma-ray and fast neutron. A linear proportional factor between the measurement of EI (proportional to thermal neutron) by the SDD and Y_n, measured by the FC, was obtained. Several research papers indicated that the polarization of the surface of SCD is induced by high dense ion beam irradiation, and this leads to the degradation of detection efficiency [34-36]. The linear proportion between the count rates by SDD and FC in Fig. 9 indicates that such polarization effect was absent in the present measurement. The absence of polarization effects in this experimental condition would be caused by the relatively low count rate and the wide window size (3.6 mm of diameter) of SDD compared to high dense ion beam

irradiation. However, the polarization effects will be emphasized in the actual fusion condition where the neutron flux is significantly high compared to this study. The influence of the polarization effects on the detection efficiency of SDD should be done in future.

Figure 10 shows a typical time evolution for a deuterium plasma discharge at LHD with electron cyclotron (EC) heating and neutral beam injection (NBI) heating (Pulse #154554). About 1 MW of total EC heating power (P_{ECH_total}) was injected into deuterium plasma. The NBI heating injection power (P_{NBI_inj}) was introduced by three NBI systems. In this pulse, the maximum total neutron emission rate (S_n) measured by FC was about 5.0×10^{14} neutrons per second. The time evolution of S_n is similar to P_{NBI_inj} as energetic deuterons originated from NBI effectively react with deuteron in plasma to produce fast neutrons. The time evolution of EI count in the SDD averaged every 100 ms is also shown in figure 10. The time evolution of the EI count reproduced quite well that from the FC. However, fluctuation is present, which is due to the relatively low S_n of this shot.

An important goal of the present study was to verify whether the SDD operated with our enhanced PSD procedure can be used for radiation safety. The high-precision measurement of thermal neutrons is important to satisfy the strict safety management plan of D-D experiment in LHD [37, 38]. Therefore, the fluctuation of the measured EI count rate was analyzed to evaluate the reliability of the measurement. The expected counts and the fluctuation of the counts as a function of time-bin were estimated by the Poisson distribution assuming the highest prescribed neutron emission rate in D-D plasma discharge for LHD, $S_n = 1.9 \times 10^{16}$ n/s. The fluctuation of count was evaluated by the standard deviation, which is the square root of the expected count in the Poisson distribution. About 95% of the counts should range within the two standard deviations (2σ). In this assumption, it was predicted that the fluctuation of EI count rate in every 100 ms acquisition time will be less than ±5%. This indicates that the SDD system with PSD method used in this work can be sufficient for the real-time radiation management issues of LHD such as evaluating the dynamic activation of vacuum vessels and components, damage in the diagnostics during long time plasma discharge, and others.

5 Conclusion

The pulse shape discrimination (PSD) technique for single crystal CVD diamond detector (SDD) was for the first time applied to real-time thermal neutron measurement during the 3rd campaign of Deuterium-Deuterium (D-D) plasma experiment in the Large Helical Device (LHD). The PSD method is based upon the different shape of electrical pulses produced by gamma-ray and energetic ions. The PSD was carried out with using

the full width at half maximum (FWHM) and the full width at 2/3 of the peak height (FW2/3PH) which reflect the difference in the pulse shape. The performance of this PSD technique was first tested by the irradiation of gamma-ray by ^{60}Co and alpha-ray by ^{241}Am radiation sources. Then, using a ^{6}LiF thermal neutron converter, a successful discrimination between gamma-rays and alpha particles and tritons generated by the ^{6}Li(n,α)^{3}H reaction induced by neutrons from ^{252}Cf spontaneous fission neutron source was demonstrated. Thanks to this PSD processing technique, the thermal neutron detection efficiency resulted approximately 1.7 times larger compared to previous measurements.

The real-time thermal neutron measurement by SDD with this enhanced PSD method was carried out during D-D plasma discharges in LHD. It was found that the time evolution of count rate of alpha particles and triton measured by SDD with PSD method reproduced well that of the fission chamber used as official LHD neutron monitor. The capability of the SDD detector using the PSD technique for the precise real-time thermal neutron measurement in LHD was demonstrated.

Acknowledgments

We would like to thank Dr. Erich Griesmayer and Dr. Christina Weiss of CIVIDEC for providing the fruitful discussion. This work is supported by the NINS program for cross-disciplinary study (Grant Number 0131190). This work is also performed with the support and under the auspices of the NIFS Collaboration Research program (NIFS19KOAA001, NIFS19KLPA001), and LHD project budget

References

[1]. M. Ishikawa, T. Nishitani, A. Morioka, M. Takechi, K. Shinohara, M. Shimada et al., First measurement of neutron emission profile on JT-60U using stilbene neutron detector with neutron-gamma discrimination, Rev. Sci. Instrum. 73 (2002) 4237.

[2]. P. van Belle, O.N. Jarvis, G. Sadler, S. de Leeuw, P. D'Hondt and M. Pillon, Calibration of the JET neutron yield monitors using the delayed neutron counting technique, Rev. Sci. Instrum. 61 (1990) 3178.

[3]. Ž. Štancar, M. Gorelenkova, S. Conroy, J. Eriksson, J. Buchanan and L. Snoj, Generation of a plasma neutron source for Monte Carlo neutron transport calculations in the tokamak JET, Fusion Eng. Des. 136 (2018) 1047.

[4]. Makoto Kobayashi, Tomoyo Tanaka, Takeo Nishitani, Kunihiro Ogawa, Mitsutaka Isobe, Akemi Kato, Takuya Saze, Sachiko Yoshihashi, Masaki Osakabe, and LHD

Experiment Group, First measurements of thermal neutron flux distribution in LHD torus hall generated by deuterium plasma experiments, Fusion Eng. Des. 137 (2018) 191–195.

[5]. T. Uda, H. Yamanishi, H. Miyake, J. Kodaira, Y. Sakuma, H. Hirabayashi, H. Obayashi, H. Yamada, O. Motojima, Radiation safety consideration for LHD experiments, J. Fusion Energy 16 (1997) 167–173.

[6]. K. Shibata, O. Iwamoto, T. Nakagawa, N. Iwamoto, A. Ichihara, S. Kunieda et al., JENDL-4.0: A new library for nuclear science and engineering, J. Nucl. Sci. Technol. 48 (2011) 1.

[7]. A. Muraro, L. Giacomelli, M. Nocente, M. Rebai, D. Rigamonti, F. Belli et al., First neutron spectroscopy measurements with a pixelated diamond detector at JET, Rev. Sci. Instrum. 87 (2016) 11D833.

[8]. D. Rigamonti, L. Giacomelli, G. Gorini, M. Nocente, M. Rebai, M. Tardocchi et al., Neutron spectroscopy measurements of 14 MeV neutrons at unprecedented energy resolution and implications for deuterium-tritium fusion plasma diagnostics, Meas. Sci. Technol. 29 (2018) 045502.

[9]. M. Pillon et. al., Experimental response functions of a single-crystal diamond detector for 5-20,5 MeV neutrons, Nucl. Instru. Meth. In phys. Res. A640 (2011) 185.

[10]. S. Almaviva, M. Marinelli, E. Milani, G. Prestopino, A. Tucciarone, C. Verona et al., Thermal and fast neutron detection in chemical vapor deposition single-crystal diamond detectors, J. Appl. Phys. 103 (2008) 054501.

[11]. M. Angelone, et. al, Thermal and fast neutron dosimetry using artificial single crystal diamond detectors, Rad. Meas. 46 (2011) 1686.

[12]. M. Pillon, et. al, Development of on-line tritium monitor based upon artificial diamond for fusion applications, IEEE Trans. Nucl. Sci. vol. 58 n.3 (2011) 1141.

[13]. M. Angelone, N. Fonnesu, A. Colangeli, F. Moro, M. Pillon, R. Villari, Calibration and test of a ^{6}LiF-diamond detector for the HCPB mock-up experiment at JET, Fus. Eng. Des. 146 (2019) 1755.

[14]. M. Angelone et. al., Development of single crystal diamond neutron detectors and test at JET tokamak, Nucl. Instrum. Meth. in Phys. Res. A595 (2008) 616.

[15]. Tengfei Du, Xingyu Peng, Zhongjing Chen, Zhimeng Hu, Lijian Ge, Liqun Hu, Guoqiang Zhong, Neng Pu, Jinxiang Chen, Tieshuan Fan, Time Dependent DD Neutrons Measurement Using a Single Crystal Chemical Vapor Deposition Diamond Detector on EAST, Plasma Sci. Technol., 18 (2016) 950-953.

[16]. Xufei Xie, Xi Yuan, Xing Zhang, Zhongjing Chen, Xingyu Peng, Tengfei Du, Tao Li, Zhimeng Hu, Zhiqiang Cui, Jinxiang Chen, Xiangqing Li, Guohui Zhang, Tieshuan Fan, Guoliang Yuan, Jinwei Yang, Qingwei Yang, Application of a single crystal chemical vapor deposition diamond detector for deuteron plasma neutron measurement, Nucl. Instrum. Methods Phys. Res. A, 761 (2014) 28-33.

[17]. Y. Takeiri, The large helical device: Entering deuterium experiment phase toward steady-state helical fusion reactor based on achievements in hydrogen experiment phase, IEEE Trans. Plasma Sci. 46 (2018) 2348.

[18]. A. Komori, H. Yamada, S. Imagawa, O. Kaneko, K. Kawahata, K. Mutoh et al., Goal and achievements of Large Helical Device project, Fusion Sc. Technol. 58 (2010) 1.

[19]. Y. Takeiri, T. Morisaki, M. Osakabe, M. Yokoyama, S. Sakakibara, H. Takahashi et al., Extension of the operational regime of the LHD towards a deuterium experiment, Nucl. Fusion 57 (2017) 102023.

[20]. Makoto Kobayashi, Kunihiro Ogawa, Mitsutaka Isobe, Takeo Nishitani, Shuji Kamio, Yutaka Fujiwara, Tomomi Tsubouchi, Sachiko Yoshihashi, Akira Uritani, Minoru Sakama, Masaki Osakabe and the LHD Experiment Group, Thermal neutron flux evaluation by a single crystal CVD diamond detector in LHD deuterium experiment, J. Instrum., 14 (2019) C09039.

[21]. P. Kavrigin, P. Finocchiaro, E. Griesmayer, E. Jericha, A. Pappalardo, C. Weiss, Pulse-shape analysis for gamma background rejection in thermalneutron radiation using CVD diamond detectors, Nucl. Instrum. Methods Phys. Res. A, 795 (2015) 88-91.

[22]. W. Shockley, Currents to Conductors Induced by a Moving Point Charge, J. Appl. Phys. 9 (1938) 635-636.

[23]. Zhong He, Review of the Shockley–Ramo theorem and its application in semiconductor gamma-ray detectors, Nucl. Instrum. Methods Phys. Res. A, 463 (2001) 250-267.

[24]. T. Williams, C. N'Diaye, D. Breton, K. Cassou, K. Dupraz, P. Favier, D. Jehanno, V. Kubytskyi, X. Liu, J. Maalmi, A. Martens, Y. Peinaud, A. Stocchi, F. Zomer, E. Griesmayer, P. Kavrigin, M.W. Ahmed, M. Sikora, H.R. Weller, Operation of a fast diamond γ-ray detector at the HIγS facility, Nucl. Instrum. Methods Phys. Res. A, 830 (2016) 391-396.

[25]. R.B. Firestone, Table of Isotopes 8th edn (New York: Wiley), 1996.

[26]. https://www.python.org/

[27]. https://cividec.at

[28]. K. Ogawa, M. Isobe, T. Nishitani, T. Kobuchi, The large helical device vertical neutron camera operating in the MHz counting rate range, Rev. Sci. Instrum., 89 (2018) 113509.

[29]. Glenn F. Knoll, Radiation Detection and Measurement 3rd edn (John Wiley), 2000.

[30]. Takeo Nishitani, Kunihiro Ogawa, Mitsutaka Isobe, Hiroki Kawase, Neng Pu, Yuri Kashchuk, Vitaly Krasilnikov, Jungmin Jo, Munseong Cheon, Tomoyo Tanaka, Sachiko Yoshihashi, Siyuan Li, Masaki Osakabe, the LHD Experiment Group, Calibration experiment and the neutronics analyses on the LHD neutron flux monitors for the deuterium plasma experiment, Fusion Eng. Des. 136 (2018) 210–214.

[31]. C. Weiss, H. Frais-Kolbl, E. Griesmayer, P. Kavrigin, Ionization signals from diamond detectors in fast-neutron fields, Eur. Phys. J. A52 (2016) 269.

[32]. Makoto I. Kobayashi, Kunihiro Ogawa, Mitsutaka Isobe, Takeo Nishitani, Teruki Nishimura, Keisuke Mukai, Sachiko Yoshihashi, and Masaki Osakabe, Design of neutron spectrum-shaping assembly around the pneumatic tube-end in the LHD torus hall for the medical research application, submitted to Plasma and Fusion Research.

[33]. M. Isobe, K. Ogawa, H. Miyake, H. Hayashi. T. Kobuchi, Y. Nakano, K. Watanabe, A. Uritani, T. Misawa, T. Nishitani, M. Tomitake, T. Kumagai, Y. Mashiyama, D. Ito, S. Kono, M. Yamauchi, Y. Takeiri, Wide dynamic range neutron flux monitor having fast time response for the Large Helical Device, Rev. Sci. Instrum, 85 (2014) 11E114.

[34]. Wataru Kada, Naoya Iwamoto, Takahiro Satoh, Shinobu Onoda, Veljko Grilj, Natko Skukan, Masashi Koka, Takeshi Ohshima, Milko Jakšic, Tomihiro Kamiya, Continuous observation of polarization effects in thin SC-CVD diamond detector designed for heavy ion microbeam measurement, Nucl. Instrum. Meth. Phy. Res. B. 311 (2014) 113-116.

[35]. C. Manfredotti, A. Lo Giudice, E. Vittone, F. Fizzotti, Y. Garino, E. Pace, Memory effects in CVD diamond, Diam. Relat. Mater., 15 (2016) 1467-1471.

[36]. A. Lohstroh, P. J. Sellin, S. G. Wang, A. W. Davies, and J. M. Parkin, Mapping of polarization and detrapping effects in synthetic single crystal chemical vapor deposited diamond by ion beam induced charge imaging, J. App. Phy., 101 (2007) 063711.

[37]. M. Osakabe, Y. Takeiri, T. Morisaki, G. Motojima, K. Ogawa, M. Isobe, M. Tanaka, S. Murakami, A. Shimizu, K. Nagaoka, H. Takahashi, K. Nagasaki, H. Takahashi, T. Fujita, Y. Oya, M. Sakamoto, Y. Ueda, T. Akiyama, H. Kasahara, S. Sakakibara,

R. Sakamoto, M. Tokitani, H. Yamada, M. Yokoyama, Y. Yoshimura, LHD Experiment Group, Current status of Large Helical Device and its prospect for deuterium experiment, Fusion Sci. Technol. 72 (2017) 199–210.

[38]. Makoto Kobayashi, Takuya Saze, Hitoshi Miyake, Kunihiro Ogawa, Mitsutaka Isobe, Masahiro Tanaka, Naofumi Akata, Kiyohiko Nishimura, Hiroshi Hayashi, Takashi Kobuchi, Mitsuhiro Yokota, Masaki Osuna, Hideya Nakanishi, Masaki Osakabe , Yasuhiko Takeiri, Radiation control in LHD and radiation shielding capability of the torus hall during first campaign of deuterium experiment, Fusion Eng. Des., 143 (2019) 180-187.

Figure captions

Fig. 1 Typical pulses induced in the SDD by alpha-ray and gamma-ray from ^{241}Am and ^{60}Co sources, respectively. The dashed lines are the interpolated data for the PSD processing. The pulse data by gamma-ray was multiplied by 2 for easy comparison to the pulse by alpha-ray.

Fig. 2 Histograms of (a) FWHM and (b) FW2/3PH of pulses induced in the SDD during the irradiation with ^{241}Am alpha-ray and^{60}Co gamma-ray

Fig. 3 The flowchart of the pulse shape discrimination (PSD) used in this work.

Fig. 4 Histogram of total charge for pulses induced by ^{60}Co gamma-ray and ^{241}Am alpha-ray irradiation in the SDD. Each histogram of the total charge induced by gamma-ray and the alpha-ray is evaluated by the PSD method.

Fig. 5 Histograms of deposited energy of pulses induced in the SDD covered with the ^{6}LiF thermal neutron converter by neutron irradiation from ^{252}Cf fission neutrons, (a) without lead (a-1: log scale, a-2: linear scale) and, (b) with 1.0 mm-thick lead insert between the SDD and the storage box of ^{252}Cf (b-1: log scale, b-2: linear scale). The histogram of all pulses are evaluated without the PSD method. The histograms of gamma-ray and EI (triton+alpha) are evaluated by the PSD method.

Fig. 6 Comparison between the deposited energy histograms for EI measured under neutron irradiation from ^{252}Cf source evaluated by only the FWHM or both FWHM and FW2/3PH.

Fig. 7 Two typical pulses induced by gamma-ray from ^{60}Co radiation source. The pulse shape is not fully triangular due to the fluctuation of the signals. (Case I) The second peak exceeds the half-maximum. The PSD method using only the FWHM judges it as a pulse due to EI. (Case II) The second peak exceeds the 2/3PH. The PSD method using only the FW2/3PH judges it as a pulse due to EI. For both of the above two cases, the enhanced PSD method developed in this work correctly evaluates them as pulses induced by gamma-ray.

Fig. 8 The deposited energy histogram for EI measured under neutron irradiation from ^{252}Cf source. The region colored by black lines can evaluate the detection of triton only. The region colored with red lines which was evaluated by the PSD method in this study can count both triton and alpha.

Fig. 9 Correlation between the EI counts evaluated by the SDD operating with the PSD method and Y_n evaluated by the FC as obtained for several tens of D-D plasma discharges in LHD (the plot refers to LHD shots from #154544 to #154700)

Fig. 10 A typical time evolution of the deuterium plasma with EC and NBI heating. The count of EI by SDD was extracted by PSD processing and averaged every 100 ms.

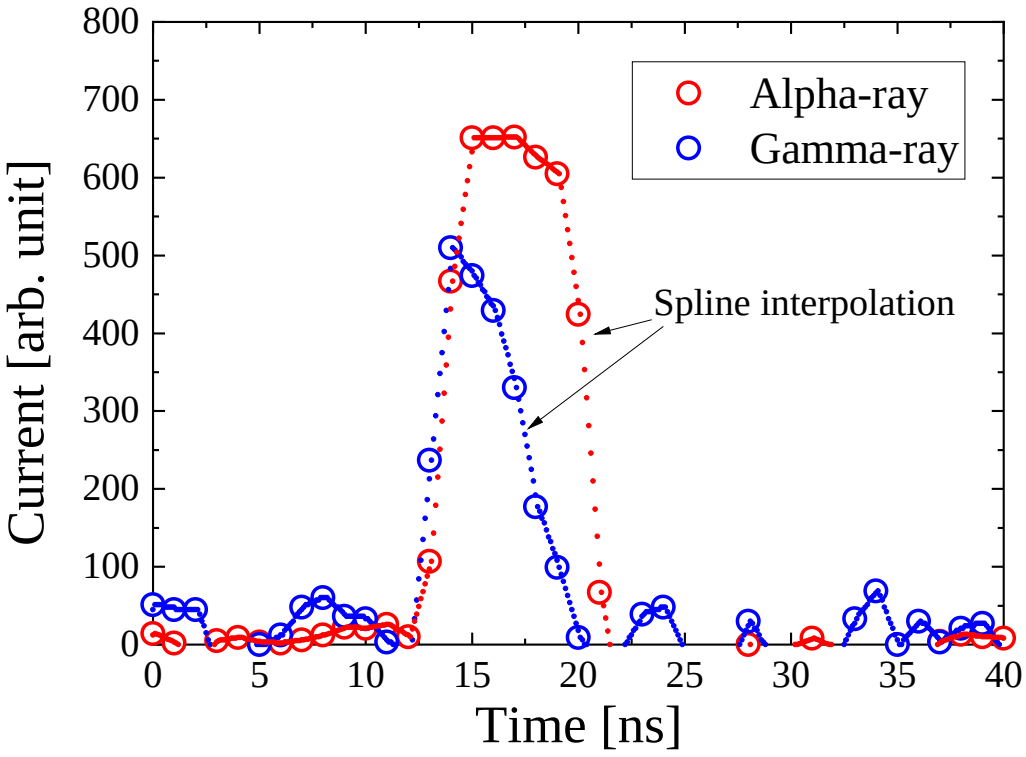

Fig.1 Makoto Kobayashi et al.

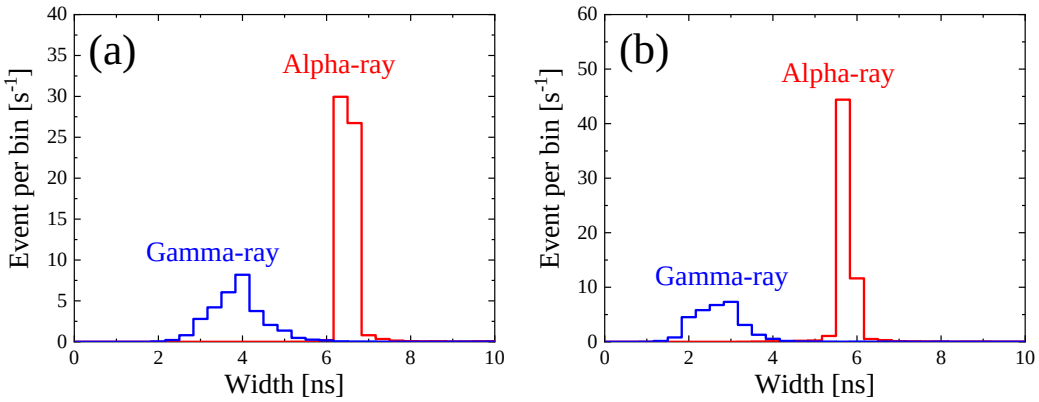

Fig. 2 Makoto Kobayashi et al

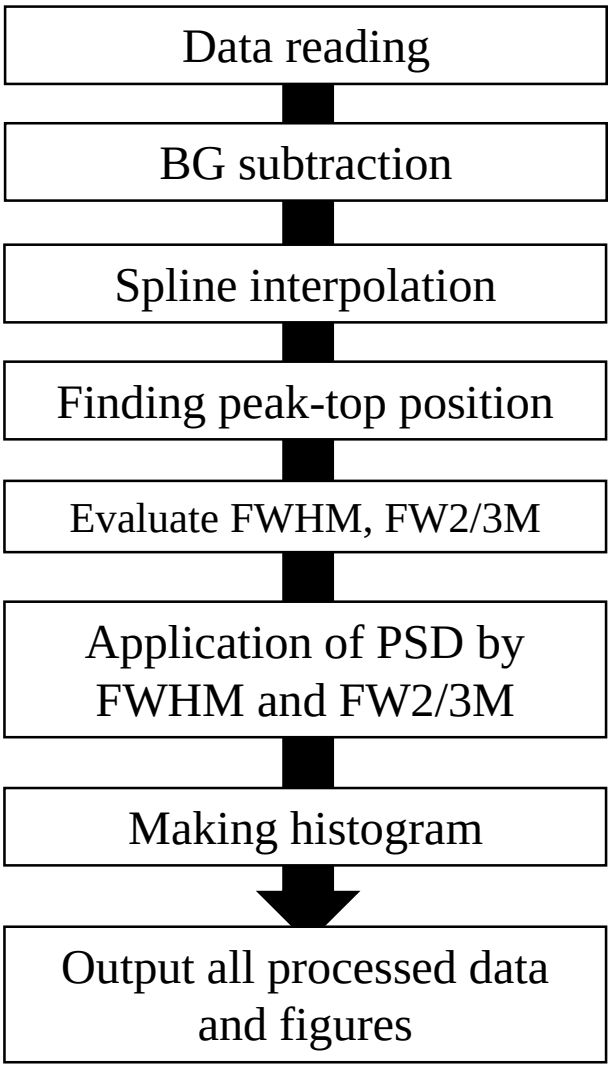

Fig. 3 Makoto Kobayashi et al

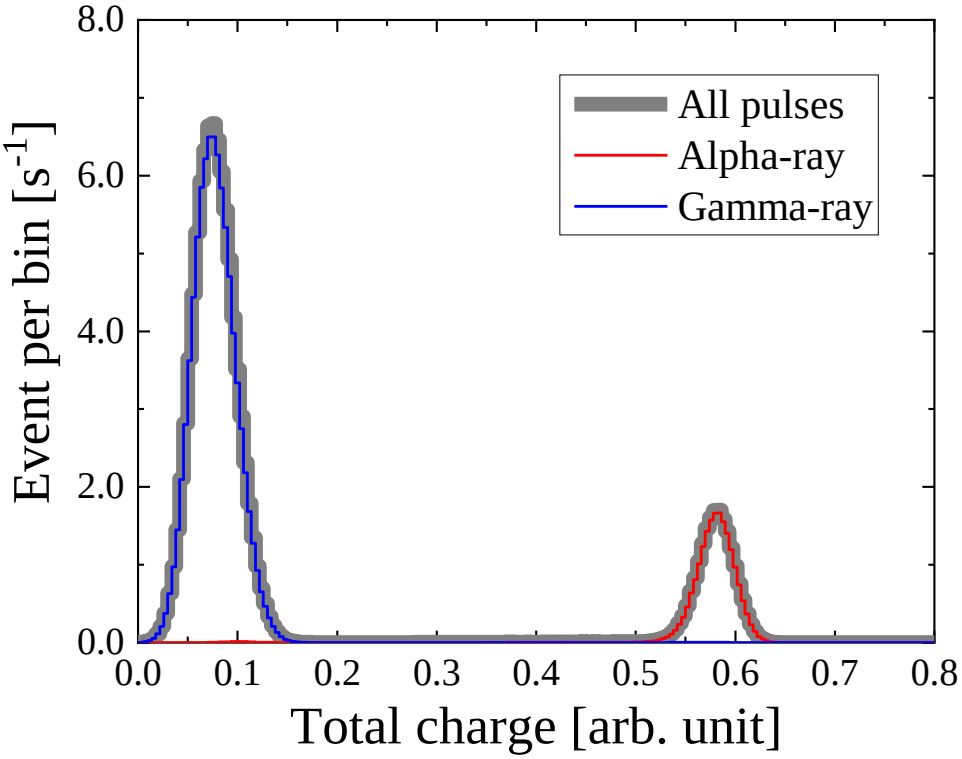

Fig. 4 Makoto Kobayashi et al

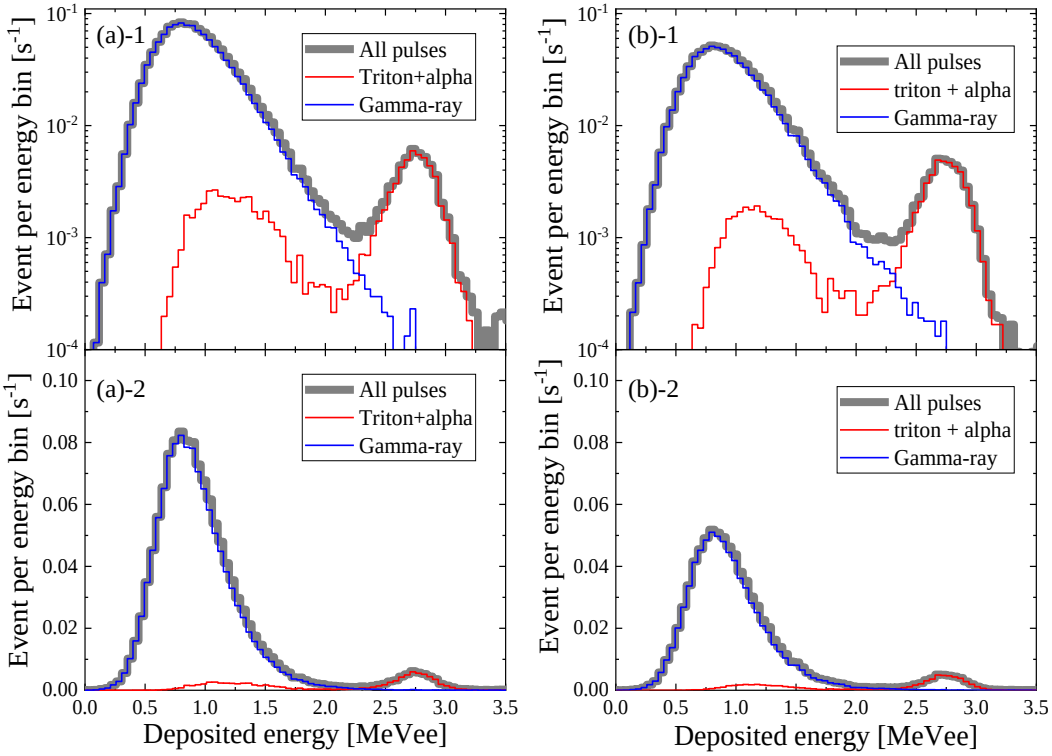

Fig. 5 Makoto Kobayashi et al.

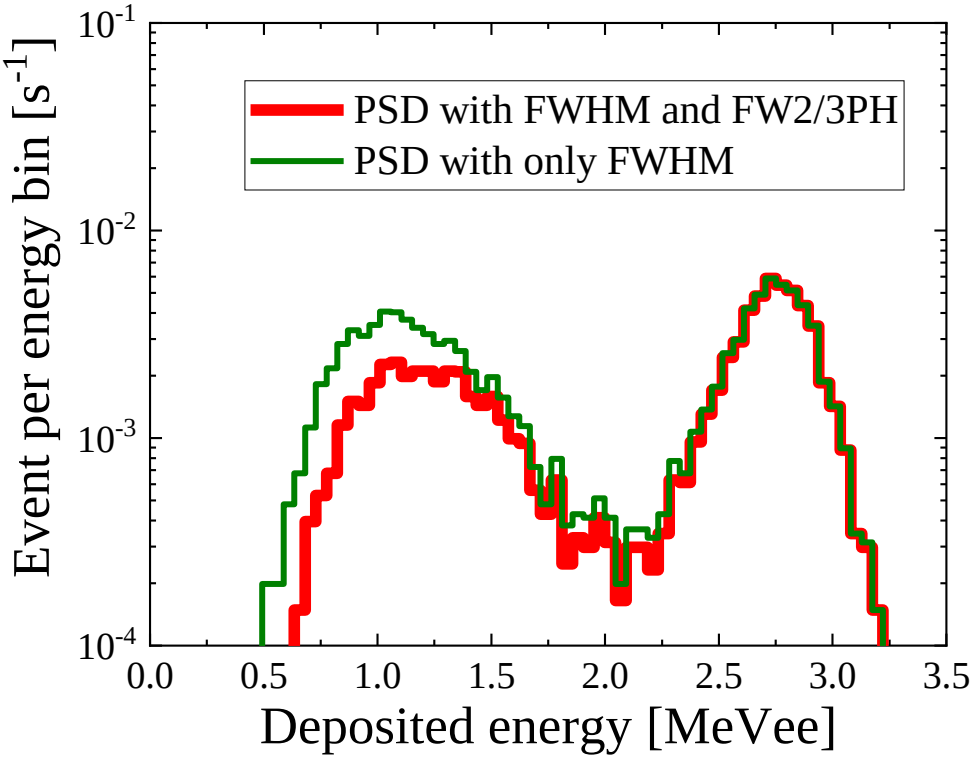

Fig. 6 Makoto Kobayashi et al.

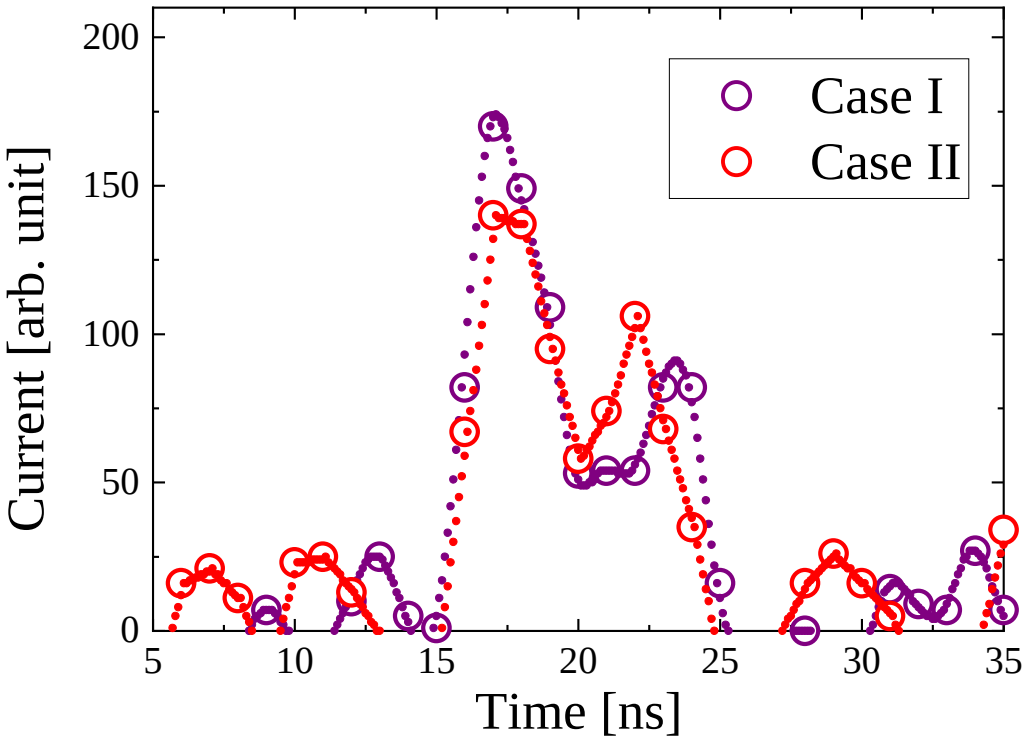

Fig. 7 Makoto Kobayashi et al.

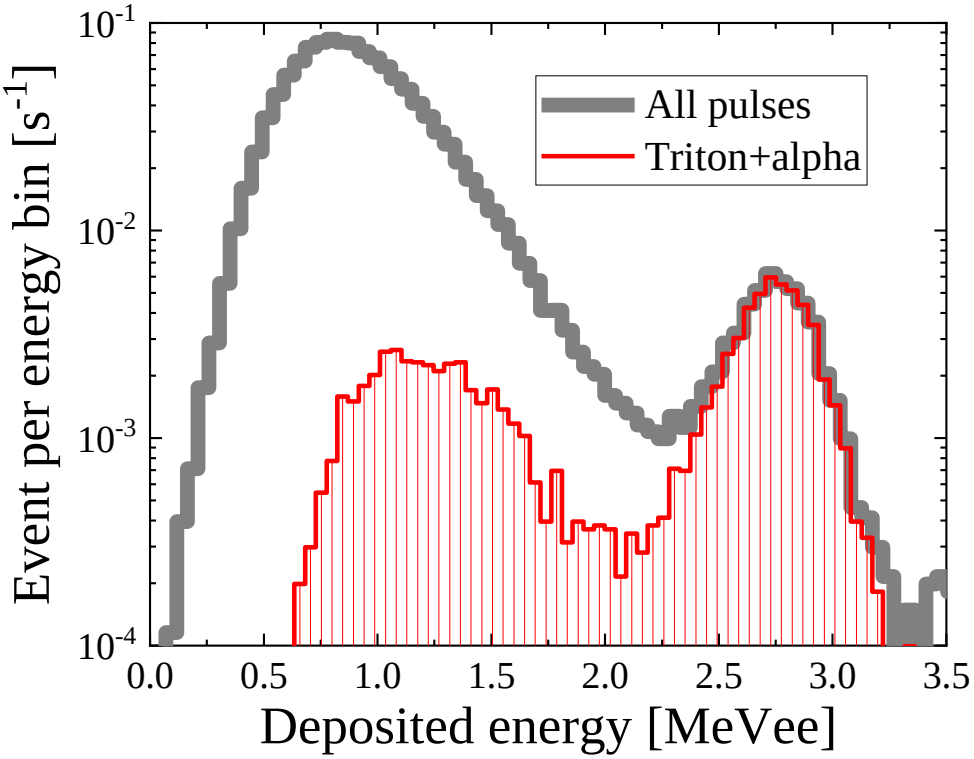

Fig. 8 Makoto Kobayashi et al.

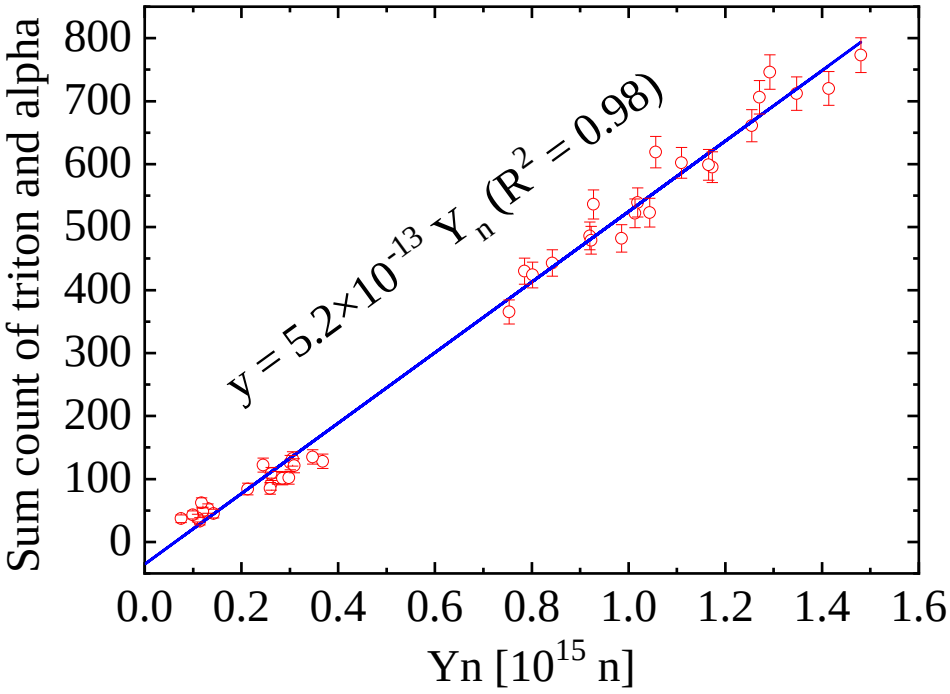

Fig. 9 Makoto Kobayashi et al.

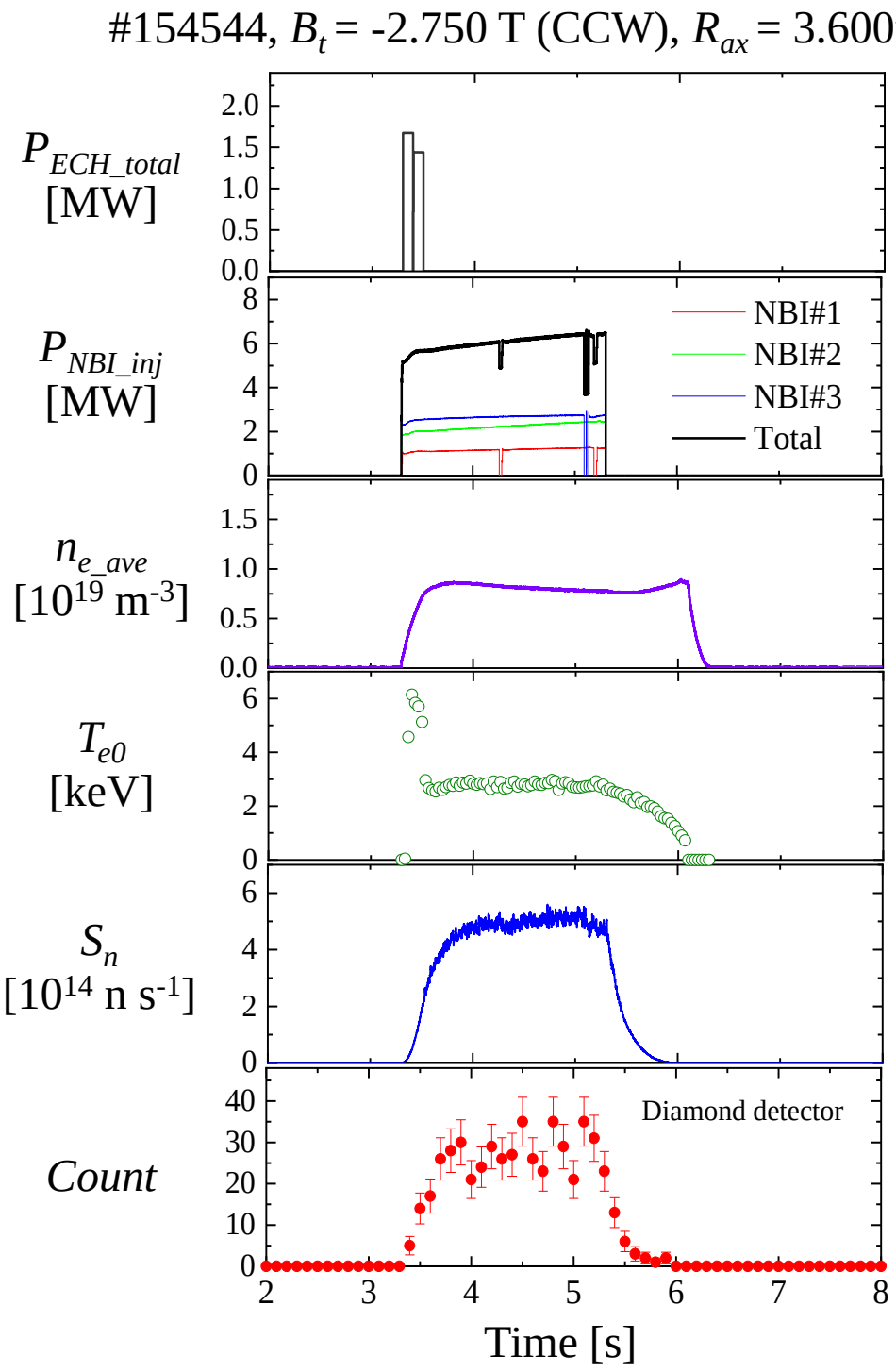

Fig. 10 Makoto Kobayashi et al.